Applied Catalysis B: Environmental 121–122 (2012) 57–64

Contents lists available at SciVerse ScienceDirect

Applied Catalysis B: Environmental

journal homepage: www.elsevier.com/locate/apcatb

A linear molecule functionalized multi-walled carbon nanotubes with well dispersed PtRu nanoparticles for ethanol electro-oxidation

Xiulin Yang[a,b], Junpeng Zheng[a,b], Mingming Zhen[a,b], Xiangyue Meng[a,b], Feng Jiang[a,b], Taishan Wang[a], Chunying Shu[a], Li Jiang[a,*], Chunru Wang[a,*]

[a] Beijing National Laboratory for Molecular Sciences, Key Lab of Molecular Nanostructure and Nanotechnology, Institute of Chemistry, Chinese Academy of Sciences, Beijing 100190, China
[b] Graduate School of Chinese Academy of Sciences, Beijing 100039, China

ARTICLE INFO

Article history:
Received 11 November 2011
Received in revised form 13 March 2012
Accepted 28 March 2012
Available online 3 April 2012

Keywords:
Multi-walled carbon nanotubes
Polyoxyethylene bis(amine)
Self-assembly
Electrocatalyst
Direct alcohol fuel cells

ABSTRACT

The performance-enhanced PtRu electrocatalysts derived from polyoxyethylene bis(amine) functionalized multi-walled carbon nanotubes (POB-MWCNTs) were fabricated by electrostatic self-assembly technology, in which Pt and Ru precursors were first uniformly distributed on the POB-functionalized MWCNT surface via the electrostatic interaction and then reduced in situ to PtRu nanoparticles in ethylene glycol-water solution. In this process, POB as the wrapping molecule not only preserves the integrity and well dispersion of MWCNTs, but also facilitates the even distribution of PtRu nanoparticles on the surface of MWCNTs. The structure and catalytic properties of the PtRu catalysts were characterized by various spectroscopic techniques such as FT-IR, Raman, TGA, XPS, TEM and XRD spectrometry, and the electrocatalytic properties for ethanol oxidation were investigated by cyclic voltammetry and chronoamperometry. It was revealed that the as-prepared PtRu catalysts possess a high electrocatalytic activity and stability for the electro-oxidation of ethanol, and it provides a facile and eco-friend approach to large-scale production of high performance fuel cell eletrocatalysts.

1. Introduction

Direct alcohol fuel cells (DAFCs) have attracted considerable attentions in recent years for their clean, mobile properties and high energy density [1,2]. Currently the fuels for DAFCs are mainly methanol, but in comparison, ethanol is more abundant, lower toxicity, and with lower permeability (but not negligible) across proton exchange membrane and higher energy density (1325.31 kJ mol^{-1}) at room temperature [3], though it usually requires higher working temperature as the ethanol electro-oxidation has to break the C—C bond of ethanol in the reaction process [4]. Undoubtedly, it remains a challenge to improve catalysts for realizing the oxidation of ethanol under low temperature [5,6].

It is well known that for fuel cells the best catalysts up-to-date are Pt-based catalysts, but Pt is usually easy to be poisoned along with the dissociated organic molecular species gradually depositing on the metal surfaces [7,8], and it would lead to sluggish anodic currents from the ethanol electro-oxidation on Pt at low temperatures. To improve the activity of catalysts for ethanol electro-oxidation, an effective way is to increase the coverage of oxygenated species (e.g., adsorbed OH), which would be vital to completely oxidize the ethanol to carbon dioxide.

Recently, it was revealed that with using the Pt—Ru alloy as catalysts, it is able to activate water mainly by the Ru part in Pt—Ru alloy, and oxidize the ethanol by the Pt part in the alloy in meantime. Moreover, the Pt—Ru alloy catalysts show high stability in acid medium and high tolerance to CO [9,10], so the Pt—Ru alloy is considered to be one of the best catalysts for DAFCs.

On the other aspect, since the last decades carbon nanotubes (CNTs) have received considerable attentions due to their unique electrical conductivity, high stability and large surface area [11,12], and they are usually taken as substrate to load catalysts with well dispersion. However, the size distribution and activity of metal catalysts on CNTs depend strongly on the surface morphology of CNTs. In general, a simple deposition of metal nanoparticles on pristine CNTs would lead to poor dispersion and low stability due to the inert chemical reactivity on CNT surfaces, so the CNTs need usually to be activated to anchor the catalytic nanoparticles before using as catalyst support [13].

The first way to activate CNTs is by some harsh oxidative processes, such as refluxing them in a mixture of HNO_3 and H_2SO_4, to generate defects on the sidewalls and tube tips of CNTs as anchor sites for further functionalizing [14,15]. The main shortcomings of this method is that both the electrical conductivity and corrosion

* Corresponding authors.
E-mail addresses: jiangli@iccas.ac.cn (L. Jiang), crwang@iccas.ac.cn (C. Wang).

0926-3373/$ – see front matter © 2012 Elsevier B.V. All rights reserved.
http://dx.doi.org/10.1016/j.apcatb.2012.03.027

resistance of CNTs would be weakened due to the high-density as-generated defects, leading to a loss of the electrochemical active surface area and a poor durability of Pt electrocatalysts during the fuel cell working [16].

The second way to activate CNTs is to non-covalently wrap the CNTs by some polymers or organic materials. The wrapping materials would provide adsorbing sites for catalysts but produce less or even no damages to the structure of CNTs [17]. For example, Star et al. reported starch-wrapped CNTs and analyzed the interaction between CNTs and starch in detail [18]. Zheng et al. discovered an effective and facile method for DNA binding to CNTs [19]. Wu et al. successfully deposited Pt and PtRu nanoparticles on MWCNTs modified by ionic-liquid polymer and the as-prepared catalysts show excellent performance in direct electro-oxidizing methanol [20]. Zhang et al. used poly(diallyldimethylammonium chloride) (PDDA) as the wrapping polymer to functionalize CNTs to load Pt nanoparticles, revealing an enhanced electrocatalytic activity towards oxygen reduction reaction [21].

In this paper, we present a facile method to wrap MWCNTs by linear molecules (POB) and then fabricate the bimetallic PtRu electrocatalysts on POB-MWCNTs via a polyol process under reflux conditions. It was revealed that the as-prepared PtRu/POB-MWCNTs catalysts not only show a uniform and size controllable PtRu nanoparticle dispersion, but also own high activity and stability for ethanol electrochemical oxidation.

2. Experimental

2.1. Materials

All chemical reagents used in this experiment are in analytical grade purity. Polyoxyethylene bis(amine) with an average molecular weight of 3350 was purchased from Aldrich. H_2SO_4, HNO_3, $H_2PtCl_6{\cdot}6H_2O$, $RuCl_3$, methanol, ethanol and ethylene glycol were used as received without further purification. The raw-MWCNTs were purchased from Shenzhen Nanotechnologies Port Co. Ltd. (Shenzhen, China) with the diameters of 20–40 nm, lengths of 5–15 μm, and purity of 95%. Vulcan XC-72 carbon black was purchased from Cabot Corporation.

2.2. POB and acid-treatment of MWCNTs

50 mg of pristine MWCNTs and 10 mg of POB were mixed and dissolved in 40 mL of ethylene glycol–water (1:1, v/v ratio), treated with sonification at room temperature for 30 min, and stirred vigorously at 120 °C for two hours, then stored at room temperature for another two days. The above solution was filtered using a nylon membrane, and washed with double-distilled water and ethanol several times to thoroughly remove those physical absorbed POB from the nanotube surfaces. The as-prepared MWCNTs were dried in a vacuum oven at 70 °C for 10 h (denoted as POB-MWCNTs). As a comparison, MWCNTs were also functionalized by a conventional acid treatment method, where the MWCNTs were first dispersed in a concentrated H_2SO_4–HNO_3 mixture (8.0 M for each acid), and placed in an ultrasonic bath to treat up at a bath temperature of 60 °C for 2 h, then the acid-treated MWCNTs were washed for several times and dried in a vacuum oven at 70 °C for 12 h (denoted as AO-MWCNTs).

2.3. Deposition of PtRu nanoparticles on POB-MWCNTs (PtRu/POB-MWCNTs)

Deposition of PtRu nanoparticles on the POB-wrapped MWCNTs (20 wt.% metal content, atomic ratio of Pt:Ru = 1:1) was achieved via polyol reduction process. Briefly, 40 mg of POB-MWCNTs with 1.78 mL of H_2PtCl_6 (18.97 mM) and 0.93 mL of $RuCl_3$ (36.31 mM) were placed in a 100 mL of round bottom flask, and 45.0 mL ethylene glycol–water solution (2:1, v/v ratio) was added. The reaction was performed under a reflux with continuous magnetic stirring condition for 4 h, and then the mixture was filtered through a nylon membrane and washed with double-distilled water and ethanol several times. The obtained PtRu/POB-MWCNTs were dried in a vacuum oven at 70 °C for 12 h. As comparing catalysts, PtRu nanoparticles on acid-treated MWCNTs (PtRu/AO-MWCNTs) and carbon black (PtRu/C) were prepared using similar procedures as described above.

2.4. Spectroscopic characterizations

Fourier transform infrared spectrometry (FT-IR) (TENSOR-27, Germany) was employed to analyze the surface chemical composition of the purified POB-MWCNTs composite, and Raman spectrometry (DXR Raman Microscope, America) was used to study the integrity and electronic structure of the samples, the weight percentage of POB to MWCNTs was determined using a thermal gravity analyzer (TGA) (STA 409 PC, Germany) with a rising temperature rate of 10 °C min^{-1} from 50 to 800 °C under continuous N_2 flow. X-ray photoelectron spectroscopy (XPS) data was recorded with an ESCALab220i-XL electron spectrometer from VG Scientific using 300 W Al Kα radiation, in which the binding energies were referenced to the C1*s* line at 284.8 eV from adventitious carbon. The morphology and microstructure of the synthesized materials were investigated by TEM (JEM-2010, Japan), X-ray diffraction (XRD) analysis was made using a Rigaku D/max2500 (Japan) diffractometer with Cu Kα radiation. The amount of Pt and Ru in each catalyst was determined by inductively coupled plasma-optical emission spectroscopy (Shimazu ICPE-9000), and prior to analysis, the catalysts were digested in aqua regia for 24 h, and then diluted to a certain concentration.

2.5. Electrochemical measurement

Electrochemical measurements were recorded using CHI660D electrochemical working station controlled by CH instrument electrochemical software, and a conventional three-electrode system was used throughout this work. The electrochemical activities of PtRu/POB-MWCNT, PtRu/AO-MWCNT and PtRu/C electrocatalysts were measured for the electro-oxidation of ethanol.

In typical process, 2.0 mg of electrocatalyst sample was mixed in 400 μL of ethanol–water solution (1:1, v/v ratio) under ultrasonic condition to form a homogeneous ink, and 5 μL of the ink was taken and dropped onto the surface of a glassy carbon electrode (GCE, with a diameter of 3 mm). Immediately, 7 μL of 1.0% Nafion solution in ethanol was added to fix the electrocatalysts on GCE surface. Pt sheet and a saturated calomel electrode (SCE) were used as the counter and reference electrodes, respectively. All potentials in the present study were given versus SCE reference electrode.

The electrochemical active surface area (EAS) was assessed using CO-stripping techniques in 0.5 M H_2SO_4 solution. Initially, the 0.5 M H_2SO_4 solution was purged by nitrogen for 15 min, then the adsorption of CO was performed by purging high-purity CO (99.9% purity) gas to the solution for 10 min while maintaining the potential at −0.16 V, and at the same potential the dissolved CO in solution was removed by bubbling nitrogen gas into the solution for 20 min. Finally, the elelctrocatalytic activity for the ethanol oxidation reaction was measured in a nitrogen-saturated 0.5 M H_2SO_4 + 1.0 M CH_3CH_2OH solution at a scan rate of 50 mV s^{-1} between −0.2 and 1.0 V. Several activation scans were performed until reproducible voltammograms were obtained, and the last cycle was used to compare the catalytic activity. The Pt metal

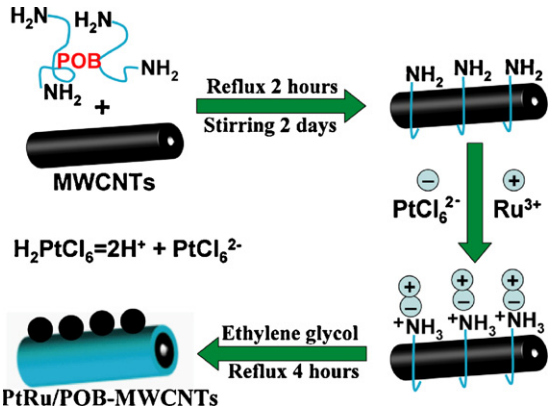

Scheme 1. Schematic diagram of the modification of MWCNTs with POB and the preparation of PtRu/POB-MWCNT catalysts.

loading was kept at 3.29 μg and all tests were conducted at ambient temperature (25 ± 0.2 °C).

3. Results and discussion

3.1. The preparation of POB-MWCNT catalysts

Scheme 1 illustrates schematically the synthesis of PtRu/POB-MWCNT catalyst. First, POB-MWCNTs were prepared simply by a reflux process where both POB molecules and MWCNTs were uniformly dispersed in ethylene glycol–water solution under ultrasonic treatment. The POB molecules tangling on the surface of MWCNTs is an entropy driven process via Van de Waals interactions between them [18]. Secondly, for the preparation of PtRu/POB-MWCNTs, it has been indicated that the POB-MWCNTs own large amounts of weakly positive charged amino groups [22], so while the precursors (H_2PtCl_6 and $RuCl_3$) was added, the negatively charged $PtCl_6^{2-}$ ions are first deposited on these positions to form nuclei, then Ru^{3+} ions were attracted driven by electrostatic force to form PtRu alloy on the surface of POB-MWCNTs.

3.2. FT-IR and Raman spectral analysis of POB-MWCNTs

As comparison, Fig. 1 displays the measured FT-IR spectra of (a) POB, (b) POB-MWCNT, (c) AO-MWCNT and (d) raw-MWCNT composites. Fig. 1a shows the IR spectrum of POB, in which the broad peak at 3431 cm^{-1} is due to the N-H stretching vibrations

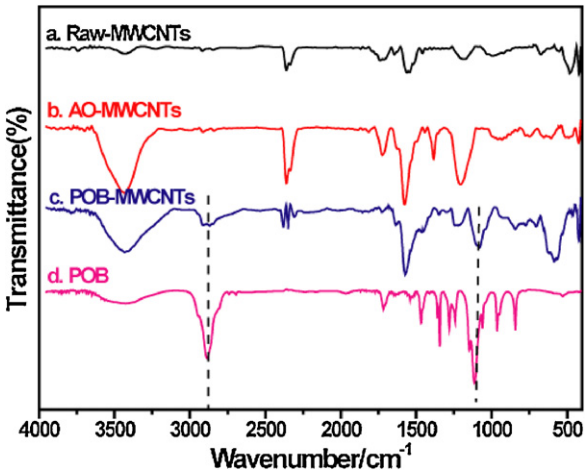

Fig. 1. FT-IR spectra of (a) POB, (b) POB-MWCNTs, (c) AO-MWCNTs and (d) Raw-MWCNTs.

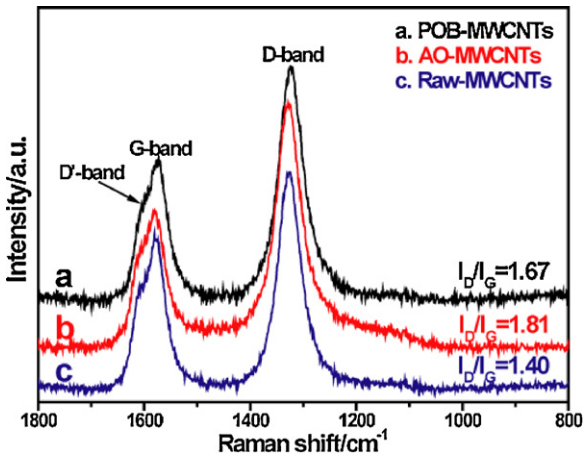

Fig. 2. Raman spectra of (a) POB-MWCNTs, (b) AO-MWCNTs, and (c) raw-MWCNTs.

[23], the peak at 2887 cm^{-1} is from the stretching of C—H [24], the peak at 1716 cm^{-1} is attributed to the C=O stretching which is also appeared in the acid treated MWCNTs in Fig. 1c, the peaks at 1531 and 1468 cm^{-1} are from the C–N and C–C asymmetric and symmetric ring stretching, respectively [25], the bands at 1344, 1281 and 1242 cm^{-1} are attributed to C–H and C–N in-plane deformation vibrations [26], the strong peak at 1115 cm^{-1} is ascribed to the C—O stretching vibration [27], the peaks located at 964 and 843 cm^{-1} are assigned to C—H out-of plane deformation [28]. For the POB-MWCNTs, Fig. 1b shows that several main absorption bands are similar to that of POB, e.g., the peaks locating at 2887 cm^{-1} (—CH_2—) and 1115 cm^{-1} (C—O—C), and the typical absorptions due to MWCNTs (Fig. 1d) are weak but also observable [23,29], confirming that the POB wraps on the surface of MWCNTs.

Raman spectroscopy is a powerful tool to characterize the crystalline degree of functionalized MWCNTs [30,31]. As shown in Fig. 2, the peak at ~1325 cm^{-1} is assigned to the A_{1g} breathing mode of disordered graphite structure (D band), the peak at ~1573 cm^{-1} is assigned to the E_{2g} stretching mode of graphite (G band), and the side band at ~1605 cm^{-1} is assigned as the D′-band [32]. Both D and D′ bands are due to defects in the hexagonal framework of graphite materials, so the height of D peak usually increases upon surface modification of carbon nanomaterials.

In fact, the number of defects in graphite materials upon surface modification can be quantified by the intensity ratio of D to G bands (I_D/I_G). As shown in Fig. 2, the ratios of peak intensity I_D to I_G are 1.40, 1.67 and 1.81 for Raw-MWCNT, POB-MWCNT, and AO-MWCNT samples, respectively. Obviously, the large I_D/I_G ratio of AO-MWCNT sample indicates more defects on the AO-MWCNTs [33] due to the harsh chemical acid treatment of MWCNTs, which would undoubtedly decrease the electrical conductivity and corrosion resistance of MWCNTs [22,34]. In contrast, the POB wrapping on MWCNTs not only preserves the integrity and electronic structure of carbon nanotubes, but also provides high effective functional groups on the surface of MWCNTs for loading the PtRu nanoparticles.

3.3. TGA analysis of POB-MWCNTs

The weight percentage of surface-bound organic moieties on CNTs can be measured by TGA analysis [35,36]. For the pristine MWCNTs (Fig. 3b), the weight loss in the temperature range of 250–700 °C is normally attributed to amorphous carbon particles (about 4.09%) attached on nanotube surfaces, but for POB-MWCNT sample, the weight loss in the same temperature range is 8.14% (Fig. 3a). The extra weight loss in POB-MWCNT sample must be

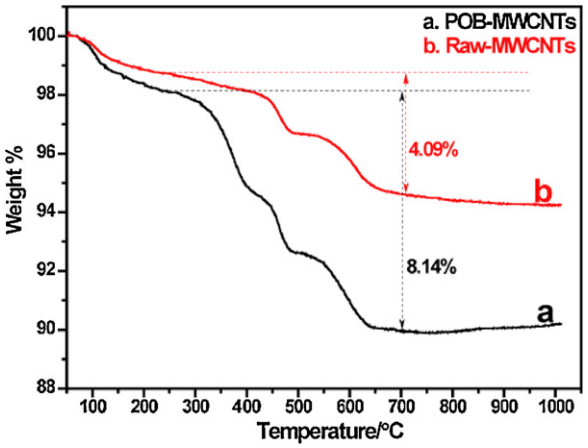

Fig. 3. TGA weight loss curves of (a) POB-functionalized and (b) pristine MWCNTs.

from the decomposition of surface modified POB moieties, which is estimated to be ca. 4.05%.

3.4. XPS analysis of PtRu/POB-MWCNTs

The XPS spectra for Pt(4*f*), Ru($3p_{3/2}$) and N(1*s*) regions of the as-prepared PtRu/POB-MWCNT nanocatalyst are shown in Fig. 4. The Pt(4*f*) region of PtRu/POB-MWCNTs shows doublet peaks due to the spin–orbital splitting as displayed in Fig. 4a, in which the intense simulating peaks with binding energies of 71.6 eV ($Pt4f_{7/2}$) and 74.9 eV ($Pt4f_{5/2}$) are attributed to the metallic Pt, and the weak simulating peaks corresponding to 72.5 and 76.0 eV are assigned to Pt^{2+} from those PtO and $Pt(OH)_2$-like species [37,38].

As the Ru(3*d*) peaks overlap with C(1*s*) peak, the Ru(3*p*) spectrum is used for the analysis of Ru oxidation state. Fig. 4b shows the Ru($3p_{3/2}$) region of the PtRu/POB-MWCNT catalyst. The Ru ($3p_{3/2}$) signal can be deconvoluted into three peaks locating at 461.9 eV, 463.2 eV and 466.6 eV, and they correspond to metallic Ru, anhydrous RuO_2, and hydrous amorphous $RuO_2{\cdot}xH_2O$ species, respectively [39,40].

Fig. 4c shows the XPS spectrum of N(1*s*), in which two peaks appearing at 399.8 and 401.3 eV indicate the presence of both free amine groups [41] and protonated ammonium ions [42,43]. Therefore, the results confirm the hypothesis in Scheme 1 that partial of the amine groups have been converted into positive charged species.

3.5. TEM and XRD analysis of PtRu/POB-MWCNTs

Fig. 5 shows the TEM images of PtRu nanoparticles on (a) POB-MWCNT, (b) AO-MWCNT and (c) carbon black catalysts, respectively. It can be observed from Fig. 5a that the POB-MWCNTs are decorated successfully with plenty of well-dispersed uniform PtRu nanoparticles with an average diameter about 2.0 nm, and no aggregated nanoparticles were shown. In contrast, for both PtRu/AO-MWCNT and PtRu/carbon-black catalysts as shown in Fig. 5b and c, metal nanoparticles disperse here and there on the MWCNTs or carbon black surfaces with a broad distribution from 1.4 to 3.8 nm.

Obviously, PtRu nanoparticles show much better dispersions on the POB-MWCNT surface than that on AO-MWCNTs or carbon black. As we already discussed before, for acid-treated nanotubes or carbon black, PtRu metals like to deposit on the defect sites on their surfaces, but it is difficult to control either the size or the position of defects on their surfaces, leading to poor dispersion and size distribution of PtRu catalysts finally. On contrary, for the POB-MWCNT catalysts, the POB film on the MWCNTs produces a uniform

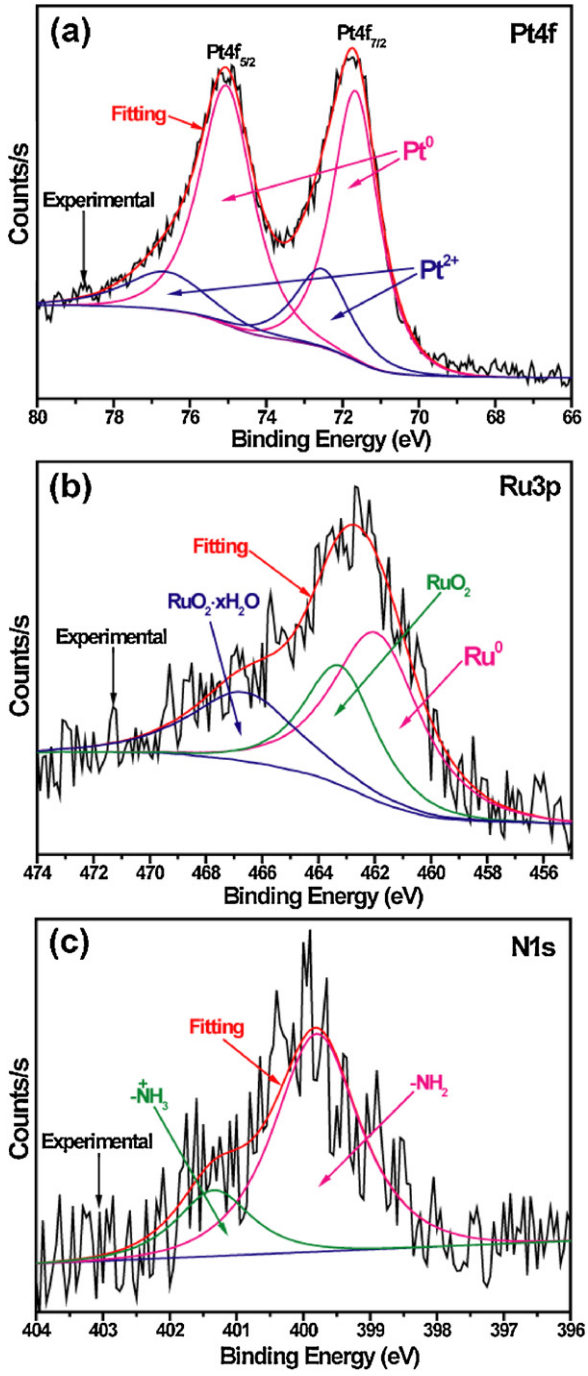

Fig. 4. XPS spectra for (a) Pt(4*f*), (b) Ru($3p_{3/2}$), and (c) N(1*s*) regions of PtRu/POB-MWCNT composite.

distribution of the amino groups that serve as active sites for adsorbing Pt and Ru precursors on the surfaces through electrostatic interaction and coordination process [21], so an uniform distribution of PtRu nanoparticles is expected.

Moreover, energy dispersive spectroscopy (EDS) analysis was performed to determine the chemical composition of the PtRu/POB-MWCNT catalyst. In Fig. 6, the elements Pt, Ru, C, O and N peaks were observed that confirms the chemical composition of the as-prepared samples.

The loading mass of PtRu nanoparticles on the POB-MWCNTs, AO-MWCNTs and carbon black can be estimated by the inductively coupled plasma-optical emission spectroscopy (ICP) as summarized in Table 1, respectively. Regarding the nanostructure of the

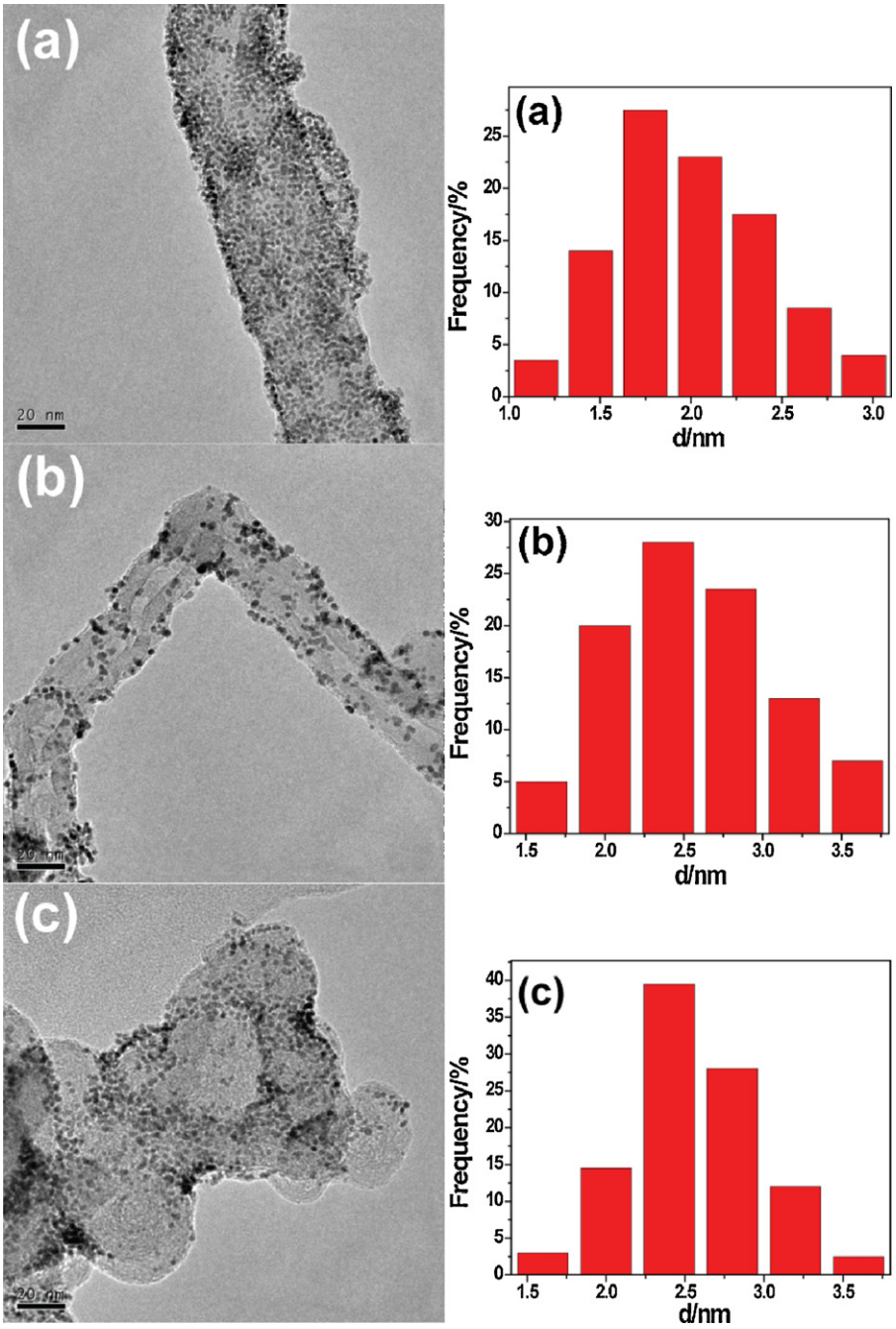

Fig. 5. TEM images of PtRu nanoparticles on (a) POB-MWCNT, (b) AO-MWCNT, and (c) carbon black catalysts.

as-prepared PtRu particles on these substrates, XRD was performed to characterize them as shown in Fig. 7, in which the broad peak at $2\theta = 26.1^\circ$ is assigned as the (0 0 2) plane of the graphite-like structure of the MWCNTs [44], and the other four characteristic peaks correspond to the (1 1 1), (2 0 0), (2 2 0), and (3 1 1) crystalline planes of the face-centered cubic (fcc) structure of Pt, respectively [45]. Comparing with XRD peaks of pure Pt (JCPDS card 04-0802), it should be noted that the four diffraction peaks for PtRu particles are shifted to high 2θ value, so the Ru must enter into Pt lattice and form PtRu alloys [46].

Table 1
The results of ICP for different PtRu alloy catalysts.

Catalysts	Pt (wt.%)	Ru (wt.%)	$n_{Pt}:n_{Ru}$
PtRu/C	13.20	5.47	1.25:1
PtRu/AO-MwCNTs	13.31	5.88	1.17:1
PtRu/POB-MWCMTs	12.96	5.69	1.18:1

Based on XRD spectra shown in Fig. 7, the PtRu particle size (d_{XRD}) and the atomic fraction of Ru in PtRu alloys (χ_{Ru}) for these carbon-supported catalysts can be estimated roughly. To estimate the average PtRu particle size d_{XRD}, Scherrer equation [35,47] was used

$$d_{XRD} = \frac{0.9\lambda}{\beta \cos\theta} \quad (1)$$

where λ is the wavelength of X-ray (0.15406 nm), θ is the diffraction angle, and β is the peak width (radians) at its half height. Here for avoiding the disturbance of carbon diffraction peak, the Pt(2 2 0) diffraction peaks in the XRD spectra were used to make the

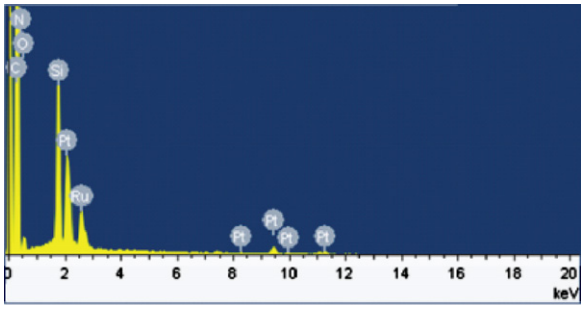

Fig. 6. EDS spectrum of the PtRu/POB-MWCNT composite.

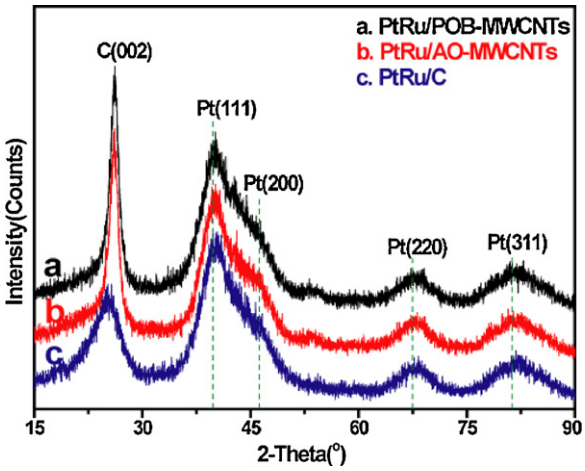

Fig. 7. X-ray diffraction patterns of the (a) PtRu/POB-MWCNTs, (b) PtRu/AO-MWCNTs and (c) PtRu/C.

calculations [48]. As shown in Table 2, the average PtRu particle sizes are calculated at 2.4, 2.5 and 1.9 nm on carbon black, AO-MWCNTs, and POB-MWCNTs, respectively.

In order to estimate the alloying degree of PtRu catalysts, the lattice parameter of Pt fcc crystal (a) was first calculated according to Vegard's law [49]:

$$a = \frac{\sqrt{2}\lambda}{\sin\ \theta} \tag{2}$$

Then χ_{Ru} can be determined according to Antolini's equation [50]:

$$\chi_{Ru} = \frac{a_0 - a}{0.0124} \tag{3}$$

where a_0 is the lattice parameter for pure platinum without Ru introducing. Because the crystallinity of small metal particles was usually affected by the nanotube curvature, the a_0 should be measured experimentally. With two Pt/C and Pt/AO-MWCNT samples prepared under same conditions, a_0 was measured as 0.3908 and 0.3922 nm on carbon black and AO-MWCNTs, respectively. As shown in Table 2, the atomic fractions of Ru in PtRu alloys are estimated as 0.2177, 0.1855, and 0.2903, respectively.

Table 2
The (2 2 0) peak, particle sizes, lattice parameter and atomic fraction of Ru for different catalysts.

Catalysts	(2 2 0) peak	d_{XRD} (nm)	a (nm)	χ_{Ru}
PtRu/C	68.27	2.4	0.3882	0.2177
PtRu/AO-MwCNTs	67.94	2.5	0.3899	0.1855
PtRu/POB-MWCMTs	68.20	1.9	0.3886	0.2903

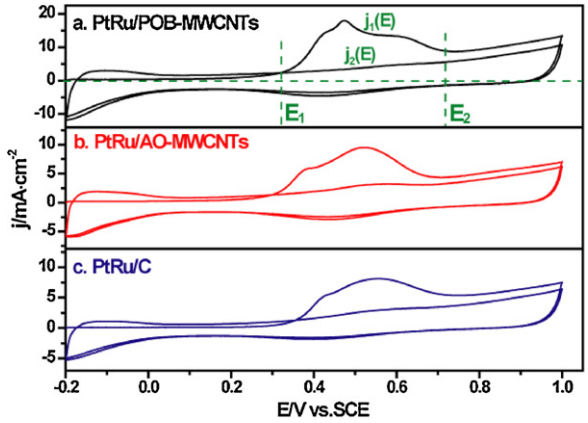

Fig. 8. CO-stripping voltammograms of (a) PtRu/POB-MWCNT, (b) PtRu/AO-MWCNT, and (c) PtRu/C catalysts in 0.5 M H_2SO_4 at room temperature and with 50 mV s^{-1} scan rate.

3.6. The electrochemical surface area of the catalysts

Fig. 8 shows the CO stripping voltammetry of the PtRu/POB-MWCNT, PtRu/AO-MWCNT and PtRu/C catalysts in 0.5 M H_2SO_4 at a scan rate of 50 mV s^{-1}, and this study was used to evaluate the EAS of the three catalysts. The adsorption time of CO was set to 10 min, since a further increase in the adsorption time did not change the slop of the curves. It can be observed from the voltammogram that for all the three catalysts, the hydrogen adsorption/desorption peaks in first scan are largely suppressed in the low potential region due to the CO adsorption saturation on the PtRu alloy surfaces [51]. Along with the potential increasing, broad peaks appear during the first scan and then disappear in the subsequent scans, indicating that the adsorbed CO species have been completely oxidized during the first forward scan.

It is well known that the CO molecules adsorb on Pt surface in a linear one-to-one bonding form. For simplicity, it is assumed that the CO molecules adopt also the linear one-to-one bonding form on surface of Pt—Ru catalysts [52], thus the EAS of these catalysts can be estimated according to following equation [5]:

$$Q_{CO} = \frac{S_{GCE}}{\nu}\left[\int_{E_1}^{E_2} j_1(E)dE - \int_{E_1}^{E_2} j_2(E)dE\right] \tag{4}$$

$$\text{EAS} = \frac{Q_{CO}}{0.42\,(\text{mC cm}^{-2})} \tag{5}$$

where S_{GCE} (0.07065 cm^{-2}) is the glassy carbon electrode surface area, ν (0.05 V s^{-1}) is the scan rate, Q_{CO} is the charge for CO desorption electro-oxidation in microcoulomb (mC), the charge to metal area conversion factor was taken as 0.42 mC cm^{-2} for Pt and Ru [4]. With this equation, the EAS for PtRu/POB-MWCNT, PtRu/AO-MWCNT and PtRu/C catalysts are calculated as shown in Table 3, in which the EAS of PtRu/POB-MWCNT catalyst is much higher than that of PtRu/AO-MWCNT and PtRu/C catalysts. Therefore, the PtRu nanoparticles depositing on POB-MWCNTs not only own uniform size and good dispersion, but also are more electrochemically active, which is very important for electrocatalysts applications in fuel cells.

3.7. Evaluation of ethanol electro-oxidation

The catalytic properties of PtRu/POB-MWCNT, PtRu/AO-MWCNT and PtRu/C catalysts for the ethanol electro-oxidation reaction have been investigated by cyclic voltammograms in 0.5 M H_2SO_4 + 1.0 M CH_3CH_2OH solution at the room temperature. Cyclic voltammograms was carried out in the potential window between

Table 3
EAS, onset potenial, peak current density and peak ratio of the different catalysts for ethanol oxidation.

Catalysts	Q_{CO} (mC)	EAS ($m^2\ g^{-1}$)	Onset potential (V)	Peak current density ($mA\ cm^{-2}$)			Peak ratio j_1/j_2
				j_1	j_2	j_b	
PtRu/C	1.60	76.2	0.47	23.02	36.11	28.65	0.64
PtRu/AO-MwCNTs	1.98	94.3	0.45	34.91	46.83	44.62	0.75
PtRu/POB-MWCMTs	2.99	142.8	0.42	53.69	59.97	51.21	0.90

−0.2 and 1.2 V at a scan rate of 50 mV s^{-1}. It can be observed in Fig. 9 that three typical ethanol oxidation peaks appear for all the three catalysts similar to those reported in literatures [53,54], in which two oxidation peaks were found during the forward sweep and the third peak was observed in backward sweep.

For PtRu/POB-MWCNT catalyst, the first and second oxidation peak (ca. 0.71 V and ca. 1.07 V, respectively) correspond largely to the formation of CO_2 and CH_3CHO as revealed by mass spectrometric cyclic voltammograms [55,56]. The third oxidation peak (ca. 0.45 V) is observed in backward sweep that is owing to the removal of those adsorbed intermediates during the ethanol oxidation process [57]. Obviously, based on the cyclic voltammograms study, the electrocatalytic activities of the three catalysts are in the following order: PtRu/POB-MWCNTs > PtRu/AO-MWCNTs > PtRu/C (see in Table 3). If we use the peak current density ratio j_1/j_2 to evaluate the conversion ability from ethanol to CO_2, the values were calculated to be 0.64, 0.75 and 0.90 for PtRu/C, PtRu/AO-MWCNTs and PtRu/POB-MWCNTs, respectively. Therefore, the PtRu catalysts loading on POB-MWCNTs show the best efficiency for oxidizing ethanol to CO_2 among the three catalysts.

Moreover, it was observed that the onset potential on ethanol oxidation is 0.42 V for PtRu/POB-MWCNT catalyst, while for PtRu/AO-MWCNT and PtRu/C catalysts the corresponding potentials are separately 0.45 and 0.47 V, as shown in Fig. 9. So PtRu/POB-MWCNT catalyst should have higher catalytic activity on ethanol oxidation due to the relative low potential comparing with PtRu/AO-MWCNT and PtRu/C catalysts.

In order to further evaluate the activity and stability of the three catalysts for ethanol oxidation, chronoamperometric measurements were performed at a constant potential (0.55 V vs. SCE) in a solution of 0.5 M H_2SO_4 + 1.0 M CH_3CH_2OH at 25 °C for 60 minutes, as shown in Fig. 10. It was revealed that although the decay current density decreases rapidly for all the catalysts due to a fast surface poisoning by adsorbed intermediates [58], PtRu/POB-MWCNT catalyst shows much higher performance than

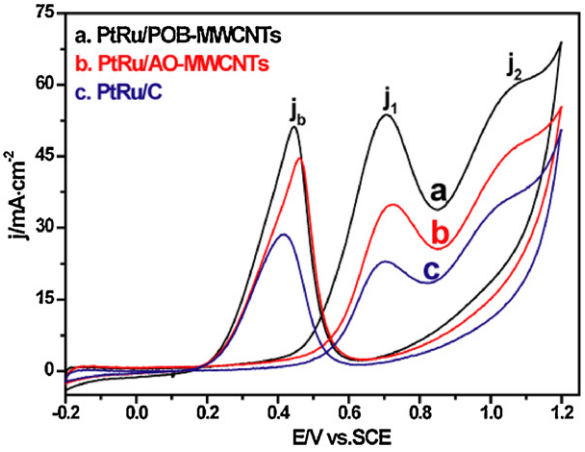

Fig. 9. Cyclic voltammograms of the (a) PtRu/POB-MWCNT, (b) PtRu/AO-MWCNT and (c) PtRu/C catalysts in 0.5 M H_2SO_4 + 1.0 M CH_3CH_2OH solution saturated by N_2 with scan rate of 50 mV s^{-1}.

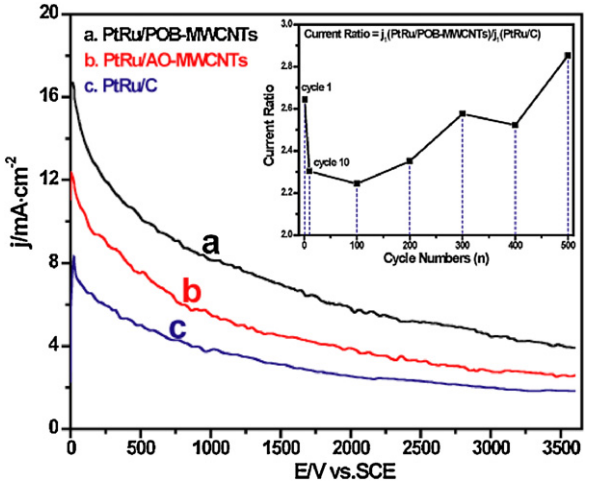

Fig. 10. Chronoamperometry collected for 60 minutes at 0.55 V for the (a) PtRu/POB-MWCNT, (b) PtRu/AO-MWCNT and (c) PtRu/C catalysts in 0.5 M H_2SO_4 + 1.0 M CH_3CH_2OH solution saturated by N_2 at room temperature. Insert figure is the first peak current density ratio of PtRu/POB-MWCNTs vs. PtRu/C at different cycle numbers.

PtRu/AO-MWCNTs and PtRu/C. As for the long-term stability of the catalysts, we performed the cyclic voltammetry measurements up to 500 cycles for PtRu/POB-MWCNTs and PtRu/C and recorded the ratio of the first peak current density of them. As shown in Fig. 10 (insert), PtRu/POB-MWCNTs catalyst shows always higher catalytic property than the contrast PtRu/C, confirming both high catalytic activity and excellent stability of PtRu/POB-MWCNTs on ethanol oxidation.

4. Conclusions

In summary, a simple and cost effective method is successfully developed to prepare an excellent catalyst for fuel cell, i.e., PtRu/POB-MWCNTs, in which the MWCNTs were first wrapped by POB molecules, and then PtRu nanoparticles were uniformly deposited on the surface POB-MWCNTs. Cyclic voltammetry and electrochemical endurance experiments indicate that PtRu/POB-MWCNT catalyst has a higher EAS from CO stripping voltammograms and better electrocatalytic activity and stability for ethanol electro-oxidation in acid solution than those PtRu nanoparticles on acid-treated MWCNTs and carbon black. These results indicated that PtRu/POB-MWCNTs would be an excellent candidate for catalysts in fuel cells.

Acknowledgements

This work is supported by the National Natural Science Foundation of China (nos. 91027108, 20821003) and National Basic Research Program (No. 2011CB933700).

References

[1] S. García-Rodríguez, F. Somodi, I. Borbáth, J.L. Margitfalvi, M.A. Peña, J.L.G. Fierro, S. Rojas, Applied Catalysis B: Environmental 91 (2009) 83–91.
[2] S. Song, J. Liu, J. Shi, H. Liu, V. Maragou, Y. Wang, P. Tsiakaras, Applied Catalysis B: Environmental 103 (2011) 287–293.
[3] H.L. Pang, J.P. Lu, J.H. Chen, C.T. Huang, B. Liu, X.H. Zhang, Electrochimica Acta 54 (2009) 2610–2615.
[4] S. Song, W. Zhou, Z. Liang, R. Cai, G. Sun, Q. Xin, V. Stergiopoulos, P. Tsiakaras, Applied Catalysis B: Environmental 55 (2005) 65–72.
[5] Z.-B. Wang, G.-P. Yin, J. Zhang, Y.-C. Sun, P.-F. Shi, Journal of Power Sources 160 (2006) 37–43.
[6] A. Kowal, M. Li, M. Shao, K. Sasaki, M.B. Vukmirovic, J. Zhang, N.S. Marinkovic, P. Liu, A.I. Frenkel, R.R. Adzic, Nature Materials 8 (2009) 325–330.
[7] J.R.C. Salgado, F. Alcaide, G. Álvarez, L. Calvillo, M.J. Lázaro, E. Pastor, Journal of Power Sources 195 (2010) 4022–4029.
[8] Y.-W. Chang, C.-W. Liu, Y.-C. Wei, K.-W. Wang, Electrochemistry Communications 11 (2009) 2161–2164.
[9] Z. Liu, X.Y. Ling, X. Su, J.Y. Lee, L.M. Gan, Journal of Power Sources 149 (2005) 1–7.
[10] G.A. Camara, R.B. de Lima, T. Iwasita, Electrochemistry Communications 6 (2004) 812–815.
[11] H. Kim, S.H. Moon, Carbon 49 (2011) 1491–1501.
[12] E. Lidorikis, A.C. Ferrari, ACS Nano 3 (2009) 1238–1248.
[13] S. Park, S.W. Yoon, H. Choi, J.S. Lee, W.K. Cho, J. Kim, H.J. Park, W.S. Yun, C.H. Choi, Y. Do, I.S. Choi, Chemistry of Materials 20 (2008) 4588–4594.
[14] L. Li, Y. Xing, Journal of Physical Chemistry C 111 (2007) 2803–2808.
[15] Y. Xing, L. Li, C.C. Chusuei, R.V. Hull, Langmuir 21 (2005) 4185–4190.
[16] J. Wang, G. Yin, Y. Shao, Z. Wang, Y. Gao, Journal of Physical Chemistry C 112 (2008) 5784–5789.
[17] D. Baskaran, J.W. Mays, M.S. Bratcher, Angewandte Chemie International Edition 43 (2004) 2138–2142.
[18] A. Star, D.W. Steuerman, J.R. Heath, J.F. Stoddart, Angewandte Chemie International Edition 41 (2002) 2508–2512.
[19] M. Zheng, A. Jagota, E.D. Semke, B.A. Diner, R.S. McLean, S.R. Lustig, R.E. Richardson, N.G. Tassi, Nature Materials 2 (2003) 338–342.
[20] B. Wu, D. Hu, Y. Kuang, B. Liu, X. Zhang, J. Chen, Angewandte Chemie International Edition 48 (2009) 4751–4754.
[21] S. Zhang, Y. Shao, G. Yin, Y. Lin, Applied Catalysis B: Environmental 102 (2011) 372–377.
[22] S. Wang, X. Wang, S.P. Jiang, Langmuir 24 (2008) 10505–10512.
[23] Y. Jalit, M.C. Rodríguez, M.D. Rubianes, S. Bollo, G.A. Rivas, Electroanalysis 20 (2008) 1623–1631.
[24] X. Zhang, J. Zhang, W. Song, Z. Liu, Journal of Physical Chemistry B 110 (2005) 1158–1165.
[25] T.-M. Wu, H.-L. Chang, Y.-W. Lin, Polymer International 58 (2009) 1065–1070.
[26] H.J. Salavagione, J. Arias, P. Garcés, E. Morallón, C. Barbero, J.L. Vázquez, Journal of Electroanalytical Chemistry 565 (2004) 375–383.
[27] D. Gonçalves, R.C. Faria, M. Yonashiro, L.O.S. Bulhões, Journal of Electroanalytical Chemistry 487 (2000) 90–99.
[28] A. Sun, Z. Li, T. Wei, Y. Li, P. Cui, Sensors and Actuators B 142 (2009) 197–203.
[29] J. Chen, M. Wang, B. Liu, Z. Fan, K. Cui, Y. Kuang, Journal of Physical Chemistry B 110 (2006) 11775–11779.
[30] A. Jorio, A.G. Souza Filho, V.W. Brar, A.K. Swan, M.S. Ünlü, B.B. Goldberg, A. Righi, J.H. Hafner, C.M. Lieber, R. Saito, G. Dresselhaus, M.S. Dresselhaus, Physical Review B: Condensed Matter 65 (2002) 121402.
[31] Y. Lin, B. Zhou, K.A. Shiral Fernando, P. Liu, L.F. Allard, Y.-P. Sun, Macromolecules 36 (2003) 7199–7204.
[32] N. Yao, V. Lordi, S.X.C. Ma, E. Dujardin, A. Krishnan, M.M.J. Treacy, T.W. Ebbesen, Journal of Materials Research 13 (1998) 2432–2437.
[33] Y. Zhao, X. Yang, J. Tian, Electrochimica Acta 54 (2009) 7114–7120.
[34] J. Li, Y. Liang, Q. Liao, X. Zhu, X. Tian, Electrochimica Acta 54 (2009) 1277–1285.
[35] Y.L. Hsin, K.C. Hwang, C.-T. Yeh, Journal of the American Chemical Society 129 (2007) 9999–10010.
[36] I. Kalinina, K. Worsley, C. Lugo, S. Mandal, E. Bekyarova, R.C. Haddon, Chemistry of Materials 23 (2011) 1246–1253.
[37] N.-Y. Hsu, C.-C. Chien, K.-T. Jeng, Applied Catalysis B: Environmental 84 (2008) 196–203.
[38] A. Velázquez-Palenzuela, F. Centellas, J.A. Garrido, C. Arias, R. María Rodríguez, E. Brillas, P.-L.s. Cabot, Journal of Physical Chemistry C 114 (2010) 4399–4407.
[39] Y. Liang, J. Li, Q.-C. Xu, R.-Z. Hu, J.-D. Lin, D.-W. Liao, Journal of Alloys and Compounds 465 (2008) 296–304.
[40] J.L. Gómez de la Fuente, M.V. Martínez-Huerta, S. Rojas, P. Hernández-Fernández, P. Terreros, J.L.G. Fierro, M.A. Peña, Applied Catalysis B: Environmental 88 (2009) 505–514.
[41] J. Sharma, S. Mahima, B.A. Kakade, R. Pasricha, A.B. Mandale, K. Vijayamohanan, Journal of Physical Chemistry B 108 (2004) 13280–13286.
[42] W.-F. Chen, J.-S. Wu, P.-L. Kuo, Chemistry of Materials 20 (2008) 5756–5767.
[43] P. Zhang, J. Li, D. Liu, Y. Qin, Z.-X. Guo, D. Zhu, Langmuir 20 (2004) 1466–1472.
[44] J. Prabhuram, T.S. Zhao, Z.K. Tang, R. Chen, Z.X. Liang, Journal of Physical Chemistry B 110 (2006) 5245–5252.
[45] Y. Bai, J. Wu, X. Qiu, J. Xi, J. Wang, J. Li, W. Zhu, L. Chen, Applied Catalysis B: Environmental 73 (2007) 144–149.
[46] Y. Chen, Y. Zhou, Y. Tang, T. Lu, Journal of Power Sources 195 (2010) 4129–4134.
[47] Z.-H. Teng, Y.-J. Wang, B. Wu, Y.-W. Tang, T.-H. Lu, Y. Gao, Applied Catalysis B: Environmental 84 (2008) 400–407.
[48] W. Zhou, Z. Zhou, S. Song, W. Li, G. Sun, P. Tsiakaras, Q. Xin, Applied Catalysis B: Environmental 46 (2003) 273–285.
[49] J. Lobato, P. Cañizares, D. Ubeda, F.J. Pinar, M.A. Rodrigo, Applied Catalysis B: Environmental 106 (2011) 174–180.
[50] E. Antolini, F. Cardellini, Journal of Alloys and Compounds 315 (2001) 118–122.
[51] F.H.B. Lima, E.R. Gonzalez, Applied Catalysis B: Environmental 79 (2008) 341–346.
[52] L. Ren, Y. Xing, Electrochimica Acta 53 (2008) 5563–5568.
[53] M.Y. Wang, J.H. Chen, Z. Fan, H. Tang, G.H. Deng, D.L. He, Y.F. Kuang, Carbon 42 (2004) 3257–3260.
[54] Z.-Y. Zhou, Z.-Z. Huang, D.-J. Chen, Q. Wang, N. Tian, S.-G. Sun, Angewandte Chemie International Edition 49 (2010) 411–414.
[55] N. Fujiwara, K.A. Friedrich, U. Stimming, Journal of Electroanalytical Chemistry 472 (1999) 120–125.
[56] Q. Wang, G.Q. Sun, L.H. Jiang, Q. Xin, S.G. Sun, Y.X. Jiang, S.P. Chen, Z. Jusys, R.J. Behm, Physical Chemistry Chemical Physics 9 (2007) 2686–2696.
[57] Z. Zhu, J. Wang, A. Munir, H.S. Zhou, Electrochimica Acta 55 (2010) 8517–8520.
[58] J.F. Gomes, B. Busson, A. Tadjeddine, G. Tremiliosi-Filho, Electrochimica Acta 53 (2008) 6899–6905.